ORIGINAL RESEARCH **Open access**

Evaluation of Remote Sensing Protocols for High-Throughput Weed Detection and Mapping

Emma Wilson[1*], Frederik De Jong[2], Lara Peters[2]

Abstract

The escalating prevalence of herbicide resistance across the United States calls for novel integrated weed management strategies that combine precise chemical deployment with non-chemical tools—using chemicals more selectively alongside non-chemical alternatives forces weeds to encounter multiple modes of action, thereby slowing the development of resistant biotypes. Yet, the generation of prescription maps and the appraisal of non-chemical tactics both hinge on field-scale weed mapping. Conventional mapping techniques entail either grueling ground-based surveys or impractical UAV imaging at low altitudes. Additionally, the published literature describes a wide range of imaging protocols that have been validated solely under narrowly defined conditions. To provide unambiguous guidance for subsequent research, the present paper contrasts three imaging modalities, two categories of weed-count models, and two ground-validation procedures (quadrat-based counts and seedbank enumeration) for remote weed mapping conducted at five locations with infestations of distinct common weed species. In summary, multispectral imaging approaches relying on Poisson count models, with quadrat weed counts serving as ground truth, outperformed alternative techniques. They may be endorsed as a workflow for expeditious weed mapping in row crops. Nonetheless, although seedbank density correlated poorly with imagery, collecting 50 seedbank samples was sufficient to characterize the seedbank.

Keywords Remote sensing, Computer vision, Weeds, UAV

*Correspondence:
Emma Wilson
emma.wilson@ed.ac.uk
[1] Department of AI-Driven Livestock Health Monitoring and Precision Feeding, Faculty of Agriculture, University of Edinburgh, Edinburgh, United Kingdom
[2] Department of Intelligent Sensor Fusion for Greenhouse Automation, Faculty of Agricultural Sciences, Wageningen University, Wageningen, Netherlands

Introduction

Heavy dependence on herbicides to suppress widespread and troublesome weed species—among them common lambsquarters (*Chenopodium album* L.), cheatgrass (*Bromus tectorum* L.), Italian ryegrass (*Lolium perenne* L. ssp. *multiflorum* (Lam.) Husnot), sterile brome (*Bromus sterilis* L.), prickly lettuce (*Lactuca serriola* L.), and wild oat (*Avena fatua* L.)—within wheat-centric cropping systems has spurred resistance to Weed Science Society of America Herbicide Groups 1, 2, 3, 4, 5, 9, 10, 14, and 15 [1-3]. Weed populations must be tackled through an integrated framework. Integrated weed management (IWM) describes a philosophy of weed suppression that draws upon a diversified toolkit, extending beyond herbicides, deployed at opportune moments and informed by weed biology. IWM tactics encompass mechanical interventions, such as harvest weed seed control [4]; cultural measures, such as cover cropping [5]; and site-specific chemical treatments [6]. Hence, a pressing need exists for in-field infestation evaluations that permit swift

This is an open access article distributed under the terms of the Creative Commons Attribution-NonCommercial-ShareAlike 4.0 International License (CC BY-NC-SA 4.0), which permits non-commercial use, distribution, reproduction, and adaptation in any medium or format, provided that appropriate credit is given to the original author(s) and source, a link to the license is provided, and any changes made are indicated. Adapted material must be distributed under the same license.

© 2022 The Author(s). | Published by Agro Intelligence Research Press

appraisal of non-chemical management measures; flag potentially herbicide-resistant patches; and yield maps enabling prescription-driven herbicide application aimed at confirmed susceptible populations.

Charting weed distributions is not a novel challenge, yet considerable uncertainty persists around benchmark techniques for efficient ground-truth data collection, particularly in remote sensing contexts. In many instances, weeds are distinguished through subjective interpretation of imagery [7]. Alternative ground truthing protocols include tallying individuals within quadrats arranged on a grid, charting single plants [8], logging presence–absence in concentric rings [9], or conducting seedbank assays [10]. Grid spacing and quadrat dimensions likewise fluctuate widely across investigations. Weed dispersion is characterized via patch margins, plant density, or seedbank density. Density typically follows a negative binomial or Poisson distribution [11] and is kriged. Selecting sampling positions demands careful planning to avoid bypassing patches whilst maintaining a feasible sample count. An efficient substitute for grid-based sampling involves adopting a nested scheme operating at disparate spatial scales [12].

UAV-based weed mapping similarly varies across flight altitude, sensor selection, and postprocessing, and scant agreement exists among these factors [7]—altitudes appearing in the literature span from under 5 m to beyond 120 m. Cameras range from off-the-shelf RGB units to multi- or hyperspectral sensors. Postprocessing stages, such as orthomosaic construction and georeferencing, may be absent or fundamental to the mapping pipeline. Predictive weed modeling in the literature includes object-oriented approaches in which crop rows and, subsequently, weeds are delineated based on image-derived features [13]. Further methods include machine learning techniques, such as k-means clustering [14], and deep learning architectures, such as YOLO v5 [15]. Newer deep learning efforts have centered on single-pass methods that employ instance segmentation but operate at altitudes too low to deliver broad-area coverage while maintaining sufficient resolution [16]. Other deep learning strategies using adapted YOLO versions produce adequate outcomes but omit reporting altitude or additional imaging parameters [17]. The area of transformer-based deep learning is still under examination for real-time weed recognition, yet deep learning as a whole demands image resolutions unattainable by UAVs flown at practical altitudes. The data volume and computational load imposed by deep learning likewise pose a barrier.

Image-derived features may include pixel-value statistics, spectral bands, vegetation indices, or morphological descriptors [18], among them the Visible Atmospherically Resistant Index (VARI), Normalized Difference Vegetation Index (NDVI), and Normalized Difference Red Edge (NDRE). The appropriateness of different models and feature sets hinges on flight altitude and ground sample distance (GSD).

Faced with an array of possible choices, researchers and growers alike may find it difficult to justify a particular weed-mapping pipeline. To guide the weed-mapping methodology throughout the ensuing years of a multi-year, multi-location investigation, this study aims to appraise contrasting ground-truth and remote-sensing mapping approaches within the PNW. To scrutinize several widely employed ground-truth and remote-sensing mapping techniques spanning a gradient of complexity, weed density was gauged via randomly positioned quadrats and grid-based seedbank sampling, performed at multiple scales and using different categories of imagery. Collectively, these datasets were examined alongside negative binomial and Poisson models employing imagery-derived features, and a judgment is rendered concerning the optimal mapping pipeline, weighed by complexity, time demand, and accuracy.

Materials and Methods

Site descriptions

During the 2023 and 2024 harvest years, five locations in the PNW were investigated, each possessing distinctive management histories, cropping sequences, and principal weed assemblages **(Figure 1; Table 1)**, though multiple species were present at every location. The 2023 experiments served as an exploratory phase to formulate a sampling framework employing only an affordable consumer-grade UAV. Five sites underwent evaluation in 2024. The heterogeneity in geographic setting, agronomic practices, climatic conditions, and weed community composition across

© 2022 The Author(s). | Published by Agro Intelligence Research Press

these locations enables rigorous assessment under a realistic array of plausible scenarios. A notable weakness of earlier weed-mapping efforts is their restriction to a single site and species, which complicates the extrapolation of methods across sites and species.

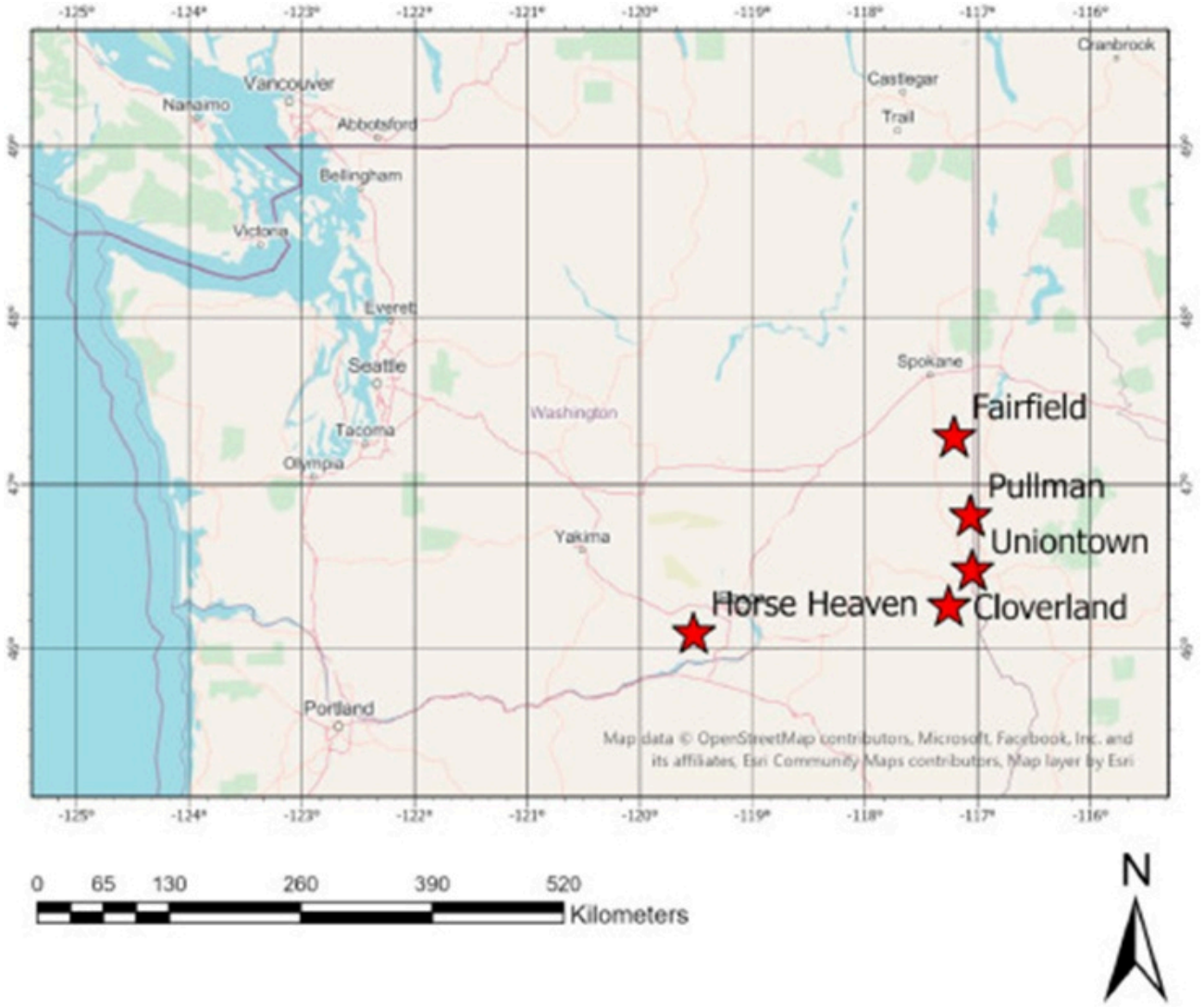

Figure 1. Location of study sites in the PNW.

Table 1. Sites examined in the study and their salient characteristics. Mean annual precipitation (MAP) from the nearest station [19]. Weeds referred to by common names: common lambsquarters (*Chenopodium album* L.), cheatgrass (*Bromus tectorum* L.), Italian ryegrass (*Lolium perenne* L. ssp. *multiflorum* (Lam.) Husnot), sterile brome (*Bromus sterilis* L.), prickly lettuce (*Lactuca serriola* L.), and wild oat (*Avena fatua* L.).

Research site	Cropping sequence	Dominant weed infestation	Plot area (ha)	Site characteristics	Annual rainfall (mm)
Horse Heaven	Winter wheat was cultivated in 2023, followed by a fallow season in 2024	Cheatgrass	5.8	Location with relatively level terrain; associated with a biopesticide experiment	222.0

© 2022 The Author(s). | Published by Agro Intelligence Research Press

Fairfield	Lentil production in 2023 and winter wheat in 2024	Common lambsquarters and prickly lettuce	2.7	Represented the study's northernmost field site	502.7
Pullman	Canola grown during 2024	Italian ryegrass	2.3	Used for investigations on weed seed suppression after harvest	526.8
Uniontown	Spring wheat established in 2024	Early-season common lambsquarters together with late-season wild oat	2.6	Included in post-harvest weed seed management assessments	318.3
Cloverland	Winter wheat production in 2024	Sterile brome	2.4	Examined under post-harvest weed seed control conditions	411.7

The Horse Heaven locale is the most arid within the investigation zone, receiving less than 250 mm of annual rainfall, and was operated under continuous no-till. The standard regional rotation is grain-fallow, where the fallow phase conserves soil moisture for subsequent wheat planting and provides opportunities for weed control during that interval. Agronomic interventions shaped the cheatgrass population throughout the imaging period. In the winter months of 2023, the parcel received an experimental dose of a biopesticide harboring *Pseudomonas fluorescens* (Battalion Pro, Bio West Ag Solutions, Caldwell, ID), together with untreated check strips. In Spring 2023, 2,4-D and metsulfuron-methyl were applied, albeit not directed at cheatgrass; later in summer, paraquat was broadcast across the field. Come spring 2024, and again during summer while the ground lay fallow, 2,4-D combined with glyphosate was administered. Within 2023, the UAV coverage zones (pink) matched the check strips plus an encircling buffer inside the field boundary; for 2024, the coverage area shifted to a 5.8 ha parcel (green) where dense weed stands had been documented the previous year. Cheatgrass reigned as the dominant species in both seasons.

The Fairfield location, lying south of Spokane, featured a conspicuous drainage swale tracing the northwestern boundary of the flight block, reduced tillage, and a triennial rotation of winter wheat, spring wheat, and a spring-sown cereal or pulse crop. Common lambsquarters was the dominant weed in a 2023 lentil stand established after a preplant glyphosate burndown. A postemergence (POST) pass of clethodim, a grass-specific herbicide, was made in 2023 to counter wild oat recorded in prior years. The 2024 winter wheat crop displayed sparse weed pressure, largely restricted to prickly lettuce during early growth stages. Common lambsquarters and grassy weeds were held in check via a POST tank mix of bromoxynil, mesosulfuron-methyl, and pinoxaden.

The Cloverland site, seeded to winter wheat, sat atop a plateau skirting the northern rim of the Blue Mountains. Its terrain was predominantly level, under no-till stewardship, and severely invaded by sterile brome. Pyroxasulfone was applied PRE in autumn 2023, followed by mesosulfuron-methyl as a POST treatment in spring 2024. This site, along with those at Pullman and Uniontown, was established to assess the performance of harvest weed seed control tactics. The Pullman site, immediately north of Pullman, WA, suffered infestations of Italian ryegrass forming well-defined clusters. Slopes were steep, and the ground received minimal tillage. Glyphosate was deployed on two occasions across the growing season. The Uniontown site, positioned south of Uniontown, WA, harbored wild oat, though the infestation remained inconspicuous early in the season, when broadleaf species instead dominated. Preplant triallate and a postemergence pinoxaden application targeted wild oat. Subsequently, after a POST glyphosate treatment, wild oat gained visibility, and common lambsquarters were brought under control.

Mapping pipelines

A suite of mapping workflows was put to the test. Two ground validation protocols (weed density surveys within quadrats and seedbank assays) were combined with three remote sensing approaches (an RGB camera flown at 30 m, a multispectral sensor operated at 60 m, and high-resolution multispectral satellite data). Weed density enumeration and seedbank quantification were chosen given their broad adoption throughout the weed science community and their

© 2022 The Author(s). | Published by Agro Intelligence Research Press

capacity to illuminate distinct dimensions of weed populations. The three imaging platforms were purposefully selected to capture a continuum of spatial detail and user accessibility—from the highest technical sophistication (i.e., multispectral) through a consumer action camera to openly available satellite scenes, which entail no expense but offer the coarsest resolution. A secondary motivation for these choices was to provide a gradient in both pixel size and spectral breadth, since conventional wisdom might suggest that richer spectral information and finer pixels would lead to improved weed-detection outcomes. In tandem, two UAV image processing environments were utilized: an open-source, no-cost package for the action camera [20], and a proprietary solution equipped with pan-sharpening functionality, Pix4Dfields [21]. **Figure 2** presents a schematic representation of the potential weed-mapping routes under examination. While superior resolution and broader spectral scope might seem inherently beneficial, we sought to uncover whether meaningful performance gaps existed and, if so, whether the results from more attainable tools were adequately comparable. Intuitively, ideal pixel dimensions would be determined by the physical size of the target weeds. The Altum-PT should be the strongest candidate for pinpointing diminutive weed specimens.

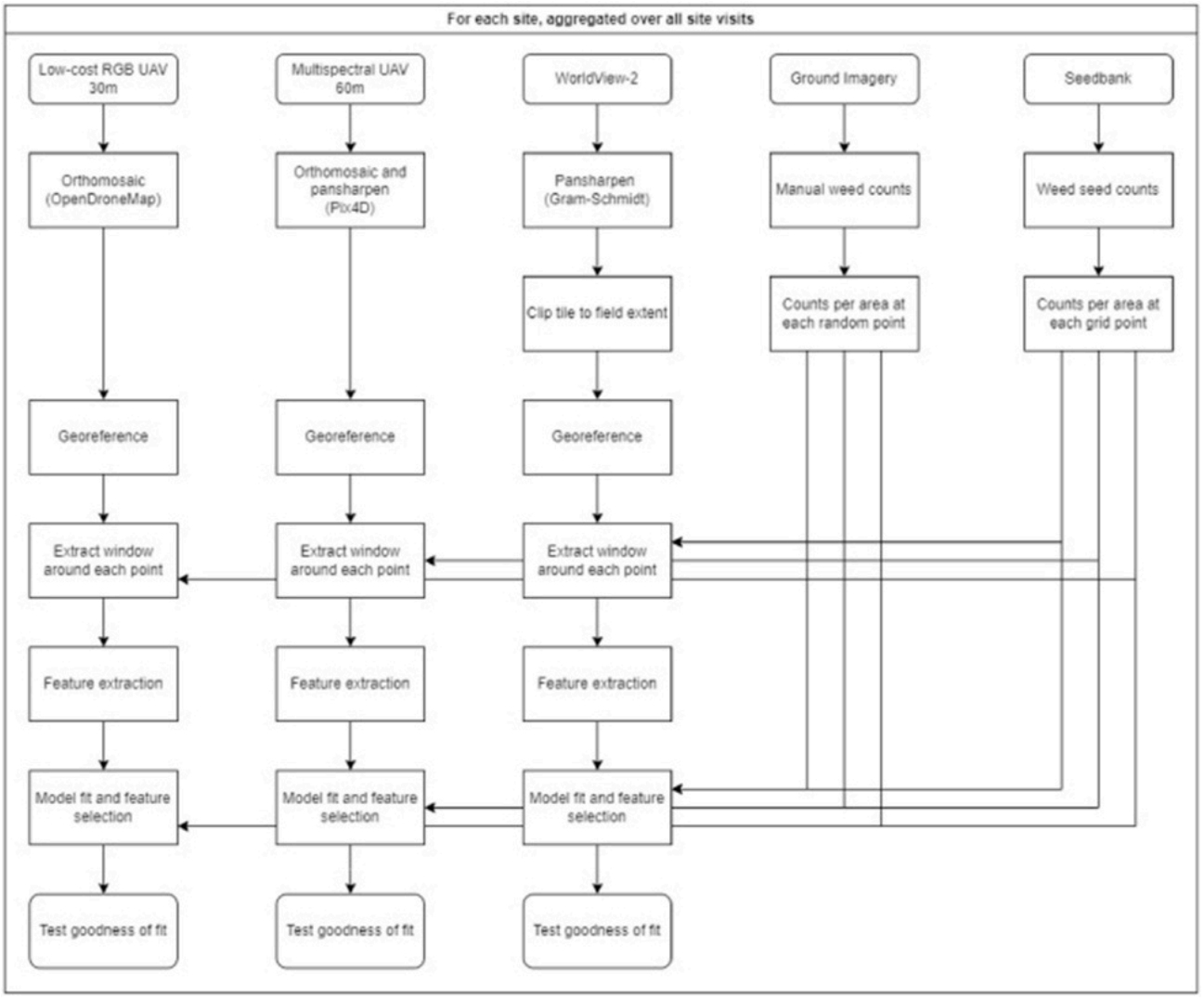

Figure 2. Processing pipelines evaluated in this study (RGB: red-green-blue, UAV: unmanned aerial vehicle).

Ground truthing and imaging methods

Weed density assessment involved designating 10 to 11 positions in a semi-random manner inside the flight zone and capturing photographs with a Canon EOS Rebel T100 [22] suspended 1.7 m overhead on a monopod, maintaining a constant 18 mm focal length. The standardized height ensured a fixed ground footprint of 2.07 m² per frame, except for a

© 2022 The Author(s). | Published by Agro Intelligence Research Press

few instances in which the lens inadvertently shifted to an alternate focal setting. Corrections for these deviations were implemented by recalculating the imaged area as needed. Points were randomly determined at the onset of the season, but allowed leeway to incorporate weed patches that materialized post-germination. In select cases, extra points were awarded for density whenever a prominent infestation patch became apparent. Such an approach mirrors a realistic scouting routine accessible to most producers. After each field excursion, species-level weed density was extracted from each photograph by manual examination and logged in the Roboflow online platform [23]. While Roboflow offers automatic annotation capabilities suited to familiar object classes or voluminous datasets, its use here was confined solely to maintaining count records. It provided a user-friendly mechanism that enabled multiple contributors to participate in image annotation. When weeds coalesced into sizeable, poorly defined clusters, most notably cheatgrass, every attempt was made to parse individual plants, though these counts likely represent underestimates. The workflow ultimately generated a species-specific weed density map anchored to the random sampling points for each field visit.

Post-harvest seedbank sampling was conducted at the Pullman, Uniontown, and Cloverland locations, employing 49–50 grid-based points within the UAV footprint. Choosing this sample size for the roughly 2.5 ha domain yielded a density of 1 point per 0.5 ha, consistent with grid intensities cited in the literature. In the absence of preliminary knowledge of weed spatial patterns, selecting an optimal grid configuration proved difficult. At each point, a soil corer with a 25.4 mm diameter was used to collect either 8 cores to a 50 mm depth or 4 cores to a 100 mm depth, subsequently stratified by depth into 50 mm layers. Uniontown was the only site where soil conditions permitted extraction to the full 100 mm; accordingly, for this paper, analysis is restricted to the upper 50 mm, albeit deeper cores might strengthen predictions where deep tillage operations occur regularly. Samples underwent elutriation with an Elutriator 48–X [24] for a 30-minute cycle, followed by air-drying overnight. Once dry, the material was hand-sieved across 0.5 mm mesh screens. A Leica dissecting microscope facilitated the removal of seeds from the residual soil matrix and debris, with identification to species level performed where possible [25, 26]. Weed seed density was expressed as the number of seeds recovered per square meter within the uppermost 50 mm of the soil profile. For this analysis, attention is narrowed to the two most prevalent weed species at each site. Rarer taxa produced an overabundance of zero counts, rendering count model fitting unfeasible.

The projected number of cores required was computed from seed density data to craft clearer sampling directives for future campaigns. The connection between the sample mean ($\bar{x}$) and the variance (s^2) conforms to a power function ($s^2 = a\bar{x}^b$), where a and b represent empirically derived parameters fitted site by site through log-transformation of the means and variances of all weed species tallies at a given location. Then, following the approach of Dessaint *et al.* [27], the retrospectively estimated necessary sample count is defined as

$$\hat{n} = a\bar{x}^{b-2}D^{-2} \quad (1)$$

Wherein a target precision (D, the ratio of s to $\bar{x}$) of 0.3 was adopted in line with Dessaint's recommendation. Evidently, a lower precision value is desirable, but Dessaint proposes 0.3 as a trade-off to keep sample numbers within practical bounds. Sample size estimation was conducted for all weed species present at each site.

Remote imaging

For remote sensing, both UAV and satellite platforms were employed. The specifications of all camera systems are compiled in. Over the course of the investigation, three UAVs were trialed, with two merged for analytical purposes. These comprised a Parrot Anafi [28] and a purpose-built quadcopter equipped with a GoPro Hero 10 Black camera [29]. The Parrot served in 2023, while the custom quadcopter replaced it in 2024 because the Parrot lacked Remote ID compliance. These platforms provide consumer-grade RGB output in JPEG format, which introduces some compression. The Parrot sensor captured 16 MP, and the GoPro 24 MP; both were flown at a height of 30 m above the highest terrain

© 2022 The Author(s). | Published by Agro Intelligence Research Press

point within each field. The third UAV, operated in 2024, was an ATI Bot V2 [30] carrying a MicaSense Altum-PT [31], a multispectral instrument equipped with blue, red, green, red-edge, near-infrared, thermal, and panchromatic detectors. Its panchromatic channel recorded 12 MP. The Altum-PT underwent calibration against a reference panel immediately before each flight. Altum-PT data were collected at 60 m above the highest elevation at every site because the sensor's electrical consumption shortened battery life. All UAV flights were conducted with 75 % overlap at a velocity of 5 m/s, roughly one hour ahead of solar noon. At each location, 4 ground control points (GCPs) were deployed and georeferenced with sub-centimeter precision at the onset of the 2024 season; during 2023, the Fairfield location possessed 5 GCPs, and Horse Heaven had 9.

UAV data followed two separate processing streams based on camera category, enabling the assessment of both free and commercial mapping software. Imagery from the consumer cameras was stitched into orthomosaics via OpenDroneMap [20], an open-source tool. The multispectral data were handled with Pix4Dfields [21], which performed pan-sharpening and orthomosaic assembly on the blue, green, red, red edge, and near-infrared channels. All camera outputs were georeferenced within ArcGIS 3.2 [32] using the surveyed GCPs at each location.

In parallel, during the 2024 season, high-resolution scenes from WorldView-2 [33] were commissioned for each site as often as possible, subject to scheduling and cloud-free conditions. WorldView-2 data deliver blue, green, red, near-infrared, and panchromatic channels, with the panchromatic band achieving roughly 0.5 m/pixel resolution, contingent on the off-nadir angle. The multispectral channels were pan-sharpened in ArcGIS employing the Gram-Schmidt algorithm [34], and the resultant sharpened product was georeferenced either to visible GCPs or, where those were indiscernible, to permanent landscape features such as utility poles.

Image processing and feature extraction

All image manipulation was carried out on the USDA SciNET high-performance computing cluster [35]. Every raster in the processed imagery collection for a given site (orthomosaicked and pan-sharpened) was matched to the temporally nearest ground quadrat assessment. Raster sampling occurred at the same geographic coordinates as the field measurements, with a 3 × 3 m sub-image extracted around each location. This dimension was chosen because the quadrats spanned approximately 1.5 × 1.5 m, and smaller cutouts yielded insufficient pixels within the 0.5 m/pixel WorldView scenes. Sub-images were screened to exclude those marred by prominent orthomosaicking defects and those where sampling points lay beyond the flight boundary. Spectral indices were derived for each sub-image, with selection determined by the available bands per image type. We selected indices that recur in the weed-imaging literature and streamlined the analysis by leveraging prior studies to discard redundant or less orthodox options [14]. The Visible Atmospherically Resistant Index (VARI) was computed for all image types; those incorporating near infrared (NIR) added the Normalized Difference Vegetation Index (NDVI); and those featuring a red-edge band further included the Normalized Difference Red Edge (NDRE):

$$\begin{aligned} \mathrm{VARI} &= (\mathrm{Green} - \mathrm{Red}) \,/\, (\mathrm{Green} + \mathrm{Red} - \mathrm{Blue}) \\ \mathrm{NDVI} &= (\mathrm{NIR} - \mathrm{Red}) \,/\, (\mathrm{NIR} + \mathrm{Red}) \\ \mathrm{NDRE} &= (\mathrm{NIR} - -\mathrm{RedEdge}) \,/\, (\mathrm{NIR} + \mathrm{RedEdge}) \end{aligned} \tag{2}$$

For each sub-image, the median and standard deviation of the indices **(Eq. 2)** were computed via Scikit-Learn's image processing toolkit in Python 3.11 [36, 37] and treated as the image-derived features. Thus, for each raster, a dataset was constructed linking weed counts per unit area for each species to image features at each sampling location, enabling calibration of a statistical count model. Rasters of the same category, originating from an identical site–crop–weed combination, were pooled. Two count model structures were investigated: Poisson and Negative Binomial, implemented through statsmodels [38] in Python. Both are conventional count frameworks within the weed science domain [11]. The

© 2022 The Author(s). | Published by Agro Intelligence Research Press

two most prevalent weed species at each site, as determined by either quadrat enumeration or seedbank assay, served as the response variable denoting predicted density, with image features as explanatory variables. Ultimately, this yielded a unique model for every combination of site, imagery category, ground truth method, and dominant weed species, fitted in both Poisson and Negative Binomial forms. Model performance was judged through Spearman's rank correlation linking observed and predicted counts, together with Akaike's Information Criterion (AIC). Moreover, for selected instances, the calibrated models were projected across entire rasters to illustrate weed mapping over more extensive areas. To gauge the relative effectiveness of different approaches, outcomes were aggregated by image category, model structure, and ground truth technique, and Spearman's rank correlation between observed and predicted counts was calculated for each grouping. Metrics such as false-positive rate, accuracy, and F1 score were deliberately omitted, as they fall under the domain of detection metrics. In contrast, the model employed here is a count model rather than a detection model. The count model estimates density rather than presence/absence, rendering detection metrics neither relevant nor applicable.

Finally, given that the ultimate aim is to deploy this technique for large-area weed mapping, the fitted models were extended over the UAV orthomosaics and the georeferenced WorldView scenes to produce continuous weed-density surfaces. The procedure imposes significant memory constraints due to image dimensions, so orthomosaics were segmented into discrete 3 m by 3 m tiles in memory, and calculations were performed using Python xarray [39]. Scrutiny of the resultant weed density rasters permitted identification of artifact origins and appraisal of fitness for herbicide prescription mapping.

Results and Discussion

Seedbank sampling assessment

Outcomes of the seedbank sampling evaluation are presented in **Table 2** and in **Figure 3**. Fitting a site-specific curve linking seedbank density variance to mean seedbank density per species ($s^2 = a\,\bar{x}^b$) yields the parameter values displayed in **Table 2**. Utilizing the span of observed weed seedbank densities ($\bar{x}$) at each location, along with the formula for estimated requisite sample count ($\hat{n} = a\,\bar{x}^{(b-2)}\,D^{-2}$), delivers the range of projected samples needed. **Figure 3** visually portrays the power-law association. For the weed species of primary concern, the estimated sample count remained below 50, indicating that the sampling effort was sufficient to secure a representative sample. For less prevalent species, e.g., catchweed bedstraw (*Galium aparine*) at the Colton location, upwards of 500 samples would be necessary.

© 2022 The Author(s). | Published by Agro Intelligence Research Press

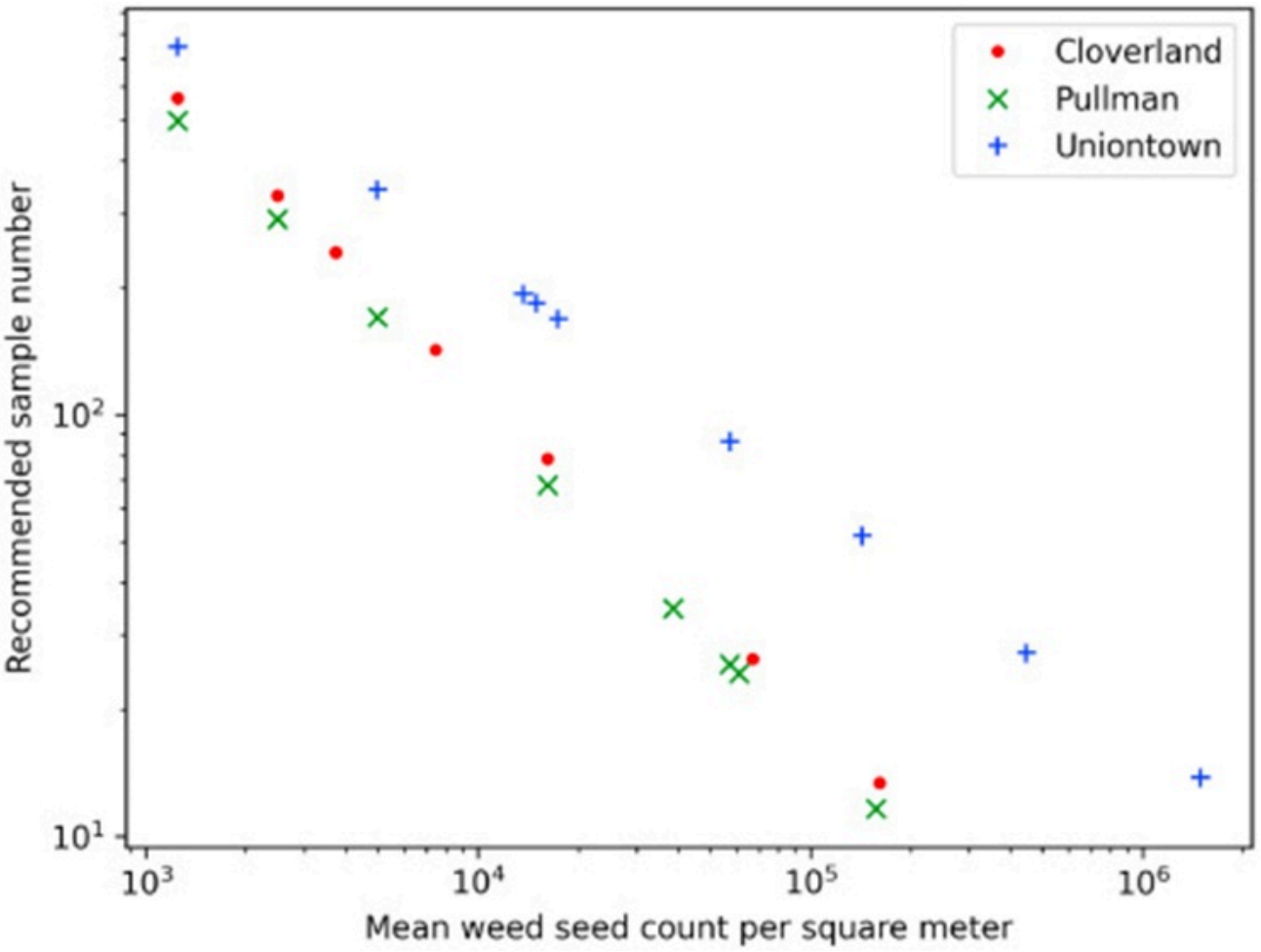

Figure 3. Estimation of the necessary total sample number (y-axis) for each site across the range of mean weed seed densities observed (x-axis). Axes are log-scaled for legibility.

Quality assessment

Imagery from the Parrot, GoPro, and Altum-PT achieved ground sample distances of <2 cm/pixel after orthomosaicking and pan-sharpening, theoretically enabling the discernment of solitary plants during early-season sorties **(Table 3)**. However, the image file format and processing workflow introduced meaningful distinctions. The JPEG files generated by the RGB cameras, despite operating at 30 m altitude, showed severe compression degradation that obscured fine detail, an issue not encountered with Altum-PT **(Figure 4, left image)**. Across both the Parrot and GoPro, JPEG quality hovered near 90 at a compression factor of 6; additionally, the GoPro's lack of gimbal stabilization worsened stitching results. Orthomosaics built with the open-source tool exhibited peculiar geometric aberrations, including warping and discontinuities, in portions of imagery from every location, as illustrated in the left panel of **Figure 4**. WorldView-2 acquisitions revealed weed clusters at Horse Heaven and Pullman. Still, the GSD proved too coarse to resolve individual plants.

In contrast, the Altum-PT workflow was the most financially demanding and called for the highest level of operational expertise. This presents a hurdle for producers, who may be disinclined to invest the time and capital necessary to procure a drone and companion software, plan and fly missions, process and interpret imagery, sustain the aircraft, and juggle multiple battery replacements to cover a workable area. A balanced, pragmatic middle ground between satellite observations and a high-resolution multispectral quadcopter payload might involve a more modest sensor fitted to a fixed-wing drone, paired with an open-source pipeline for converting imagery into weed maps. Environmental conditions during

© 2022 The Author(s). | Published by Agro Intelligence Research Press

image capture could pose an additional obstacle. In this work, acquisitions were made only under pristine, cloudless, still-air conditions; however, in certain regions, the period requiring weed maps may overlap with a season when inclement weather precludes suitable flight windows. For weed science research objectives, scheduling may afford greater flexibility, and the premium instrumentation could warrant the associated cost and labor.

Table 2. Results of seedbank sampling assessment. a, b, and n̂ are from Dessaint *et al.* [27], in the equation for sample variance ($s^2 = a\,x_^{b}$) and sample number ($\hat{n} = a\,x_^{b-2D-2}$).

Site	*n̂* range	b	a
Cloverland	(12.39, 564.41)	1.23	12,132.50
Pullman	(25.55, 497.99)	1.22	11,264.08
Uniontown	(13.80, 745.78)	1.44	3692.43

Table 3. Image characteristics for acquisition systems employed over several field sites and years to quantify aboveground weed density (RGB: red-green-blue, NIR: near infrared, Pan: panchromatic).

Parameter	Parrot sensor	GoPro camera	Altum-PT system	WorldView-2 satellite
Final ground sampling distance (m/pixel)	0.011	0.012	0.014	0.429
Spectral configuration	RGB channels	RGB channels	Blue, green, red, red-edge, near-infrared, thermal, and panchromatic bands	RGB with NIR and panchromatic bands
Output file type	JPEG	JPEG	TIF	NTF
Compression setting (quality level)	90 (6)	92 (6)	Not applicable	Not applicable
Gimbal support	Available	Not available	Available	Not applicable
Operating/Flying height (m)	30	30	60	770,000
Spatial resolution (pixel dimensions)	4608 × 3456	5568 × 4176	Multispectral imagery: 2064 × 1544; Thermal imagery: 320 × 256; Panchromatic imagery: 4112 × 3008	Not available

© 2022 The Author(s). | Published by Agro Intelligence Research Press

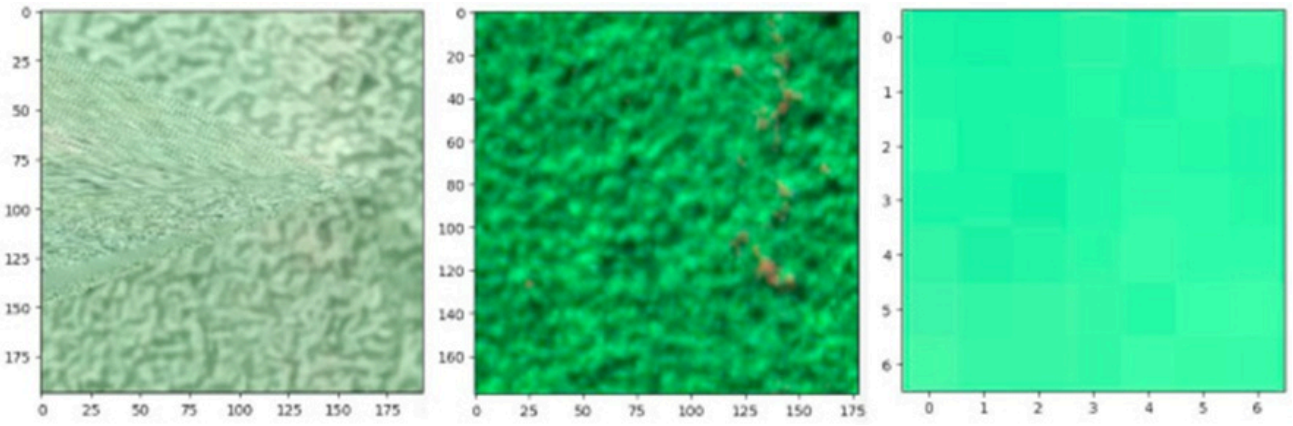

Figure 4. From left to right: GoPro, Altum-PT, and WorldView-2 images from the Pullman site at one quadrat sample location. Axes ticks are pixel numbers.

Count the model's performance

Figure 5 depicts how distinct camera systems and model structures (negative binomial and Poisson) performed across various weed species when calibrated against quadrat-count ground truth data. In general, predictive power peaked for Italian ryegrass and cheatgrass under Altum-PT (R = 0.7782 and R = 0.8874 for Italian ryegrass and cheatgrass, respectively) and WorldView-2 imagery (R = 0.6401 and R = 0.7863 for Italian ryegrass and cheatgrass, respectively). This outcome is noteworthy because both species formed expansive, well-defined clusters easily picked up by multispectral sensors, as highlighted in **Figure 6**. Weed taxa that aggregate into dense stands or possess spreading architectures appear most amenable to detection, owing to their greater spatial coverage and visual departure from planted crop rows. Despite this, the RGB cameras consistently underperformed, likely due to compression-induced degradation **(Figure 4)** and the lack of additional spectral bands. Remaining weed species never coalesced into substantial patches, rendering them far less conspicuous and compressing the observed count range. Both the negative binomial and Poisson frameworks turned in respectable results. **Table 4** catalogs the test statistics for these identical models, relaying a broadly congruent message, though Poisson specifications edged ahead on Spearman rank correlation. AIC figures were higher for Poisson fits in many—though not all—instances, suggesting a lower likelihood that the Poisson form is the superior choice. Operationally, the negative binomial should be preferred whenever overdispersion is present, since the Poisson model imposes equality between the mean and the variance. Overdispersion is the norm with clustered or patchy weed distributions. When weeds exhibit such spatial structuring, sampling grids must be configured with a spacing finer than the patch dimensions to ensure capture. Remote sensing GSD becomes less of a limiting factor for patch-forming species, considering the cluster dimensions observed in this study were discernible across both coarse- and fine-resolution sensors. Conversely, weed species that stay small and occur as scattered individuals may demand higher-resolution imagery with GSD smaller than the plant's physical span.

© 2022 The Author(s). | Published by Agro Intelligence Research Press

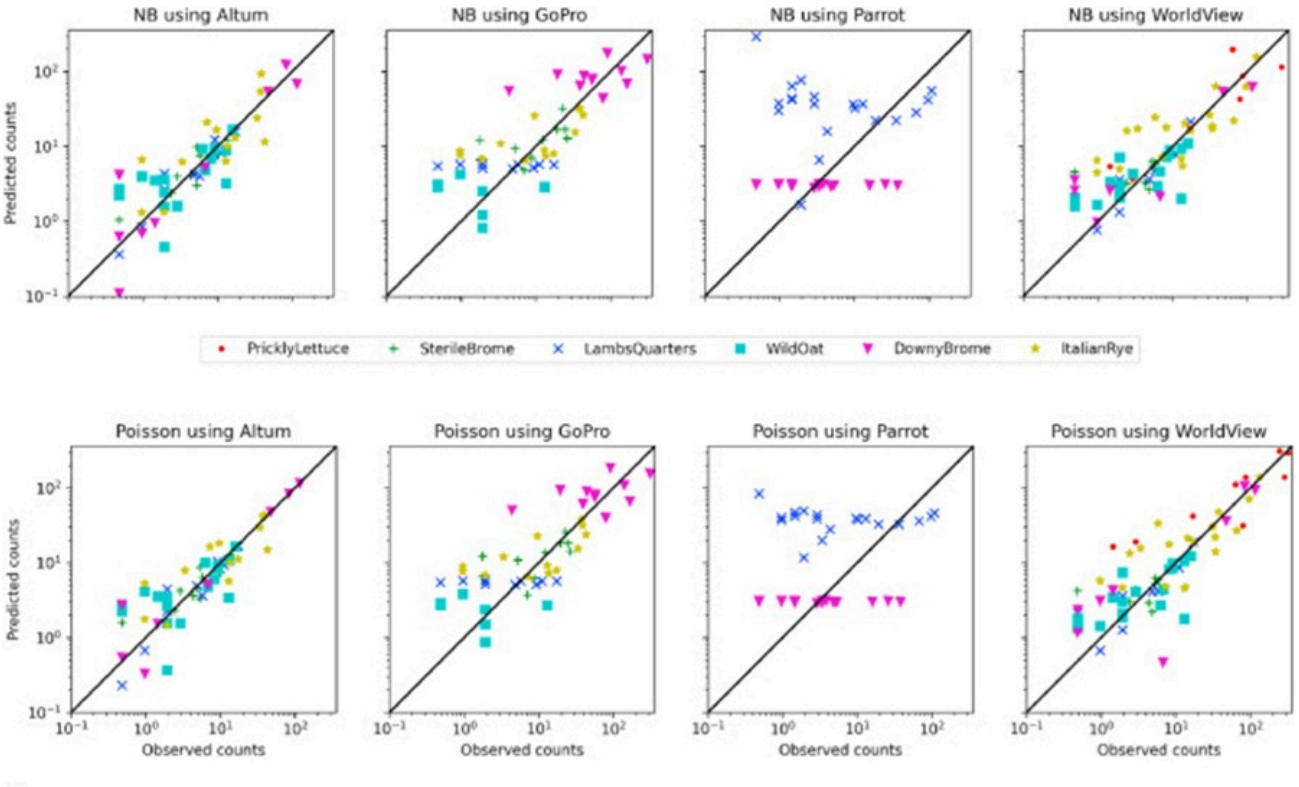

Figure 5. Prediction performance for different weeds, cameras, and count models using quadrat weed density assessments (NB: negative binomial). The top row uses the NB model; the bottom row uses the Poisson model. Each column corresponds to a camera type. Weeds referred to by common names: common lambsquarters (*Chenopodium album* L.), cheatgrass (*Bromus tectorum* L.), Italian ryegrass (*Lolium perenne* L. ssp. *multiflorum* (Lam.) Husnot), sterile brome (*Bromus sterilis* L.), prickly lettuce (*Lactuca serriola* L.), and wild oat (*Avena fatua* L.).

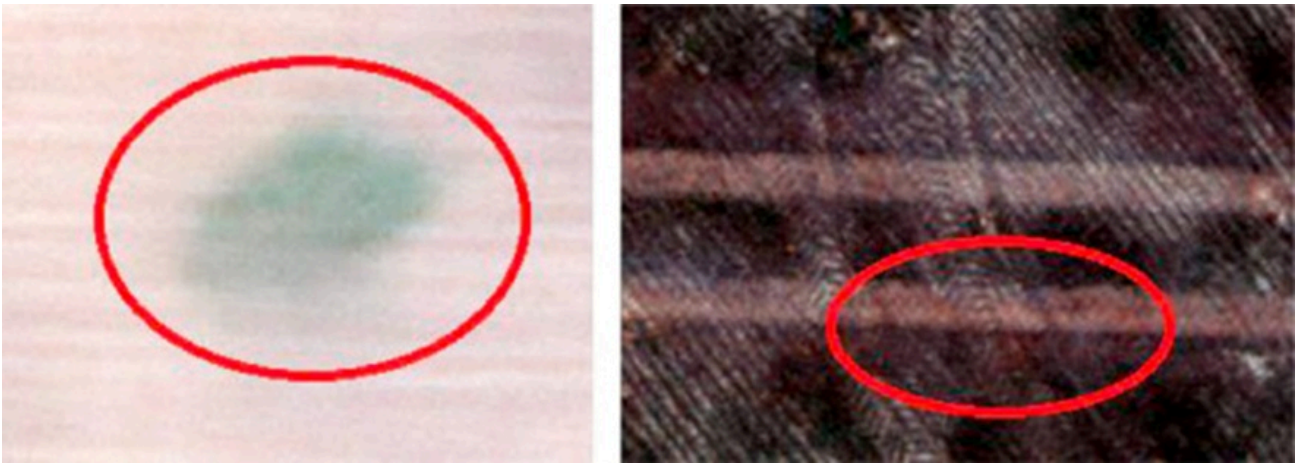

Figure 6. Weeds patches, circled in red. Left: Italian ryegrass (*Lolium perenne* L. ssp. *multiflorum* (Lam.) Husnot) patch with WorldView-2. Right: Cheatgrass (*Bromus tectorum* L.) patch with Altum-PT.

Table 4. Model performance for different sites, cameras, and model types, with quadrat counts as ground truth.

Location	Sensor platform	Target weed species	Poisson model AIC	Poisson model (R)	NB model AIC	Negative binomial model (R)

© 2022 The Author(s). | Published by Agro Intelligence Research Press

Cloverland	Altum	Sterile brome	52.5285	0.8450**	66.6712	0.8571**
Cloverland	GoPro	Sterile brome	83.6009	0.6869*	75.6529	0.7538*
Cloverland	WorldView	Sterile brome	52.7552	0.7720**	64.1308	0.7720**
Fairfield	Altum	Prickly lettuce	348.0933	0.7939**	109.9345	0.8909***
Fairfield	GoPro	Prickly lettuce	831.9847	0.6000(ns)	115.1790	0.5636(ns)
Fairfield	Parrot	Common lambsquarters	2384.1862	−0.1998(ns)	195.7944	−0.2018(ns)
Fairfield	Parrot	Prickly lettuce	162.6575	0.1256(ns)	79.5797	0.1316(ns)
Fairfield	WorldView	Prickly lettuce	359.0690	0.9273***	101.6813	0.8667**
Horse Heaven	Altum	Cheatgrass	53.0999	0.8368**	67.6165	0.8874***
Horse Heaven	GoPro	Cheatgrass	604.8106	0.4146(ns)	125.6403	0.4146(ns)
Horse Heaven	Parrot	Cheatgrass	414.4257	0.0124(ns)	182.4808	−0.0112(ns)
Horse Heaven	WorldView	Cheatgrass	104.9478	0.6345*	68.2702	0.7863**
Pullman	Altum	Italian rye	163.0264	0.7406**	112.9357	0.7782***
Pullman	GoPro	Italian rye	194.1679	0.5083(ns)	107.3011	0.5127(ns)
Pullman	WorldView	Italian rye	322.9354	0.6055**	164.8179	0.6401**
Pullman	WorldView	Prickly lettuce	17.6198	0.4914*	18.4423	0.4914*
Uniontown	Altum	Common lambsquarters	49.3033	0.9174***	62.9857	0.9146***
Uniontown	Altum	Wild oat	109.9879	0.7550***	110.2115	0.7498***
Uniontown	GoPro	Common lambsquarters	82.5780	−0.2393(ns)	61.9733	−0.1657(ns)
Uniontown	GoPro	Wild oat	61.0883	0.2244(ns)	42.8538	0.2244(ns)
Uniontown	WorldView	Common lambsquarters	46.6528	0.9174***	59.6061	0.9174***
Uniontown	WorldView	Wild oat	130.4922	0.5914**	112.7805	0.5659**

*** = P < 0.001; ** = P < 0.01; * = P < 0.05, (ns) = not significant; NB = negative binomial. Weeds referred to by common names: common lambsquarters (*Chenopodium album* L.), cheatgrass (*Bromus tectorum* L.), Italian ryegrass (*Lolium perenne* L. ssp. *multiflorum* (Lam.) Husnot), sterile brome (*Bromus sterilis* L.), prickly lettuce (*Lactuca serriola* L.), and wild oat (*Avena fatua* L.).

Table 5, together with **Figure 7**, summarizes model behavior when the seedbank provided the ground truth reference. Correlational strength declined, and AIC values rose relative to quadrat-based ground truthing. Sterile brome matched with WorldView and lambsquarters paired with Altum-PT yielded the highest performance. The generally poorer capacity

© 2022 The Author(s). | Published by Agro Intelligence Research Press

of seedbank metrics to forecast aboveground weed abundance may reflect management-driven effects [40], species-specific reproductive strategies, or soil characteristics that govern the coupling between surface vegetation and the buried seed pool. To illustrate, field sections where crop stands faltered supported denser sterile brome infestations; such sections were visually prominent in WorldView scenes. Although these areas did not explicitly display weeds in the satellite imagery, their spectral and textural signatures proved detectable at that resolution. These thin crop zones would persist across seasons, steadily amassing larger seed banks through repeated, unimpeded seed return. About common lambsquarters, each plant's prodigious seed output means patches can accumulate extraordinarily dense seedbanks, and published work has documented tighter spatial alignment between surface-level and subsurface populations for this species relative to grassy weeds [41].

Table 5. Model performance for different sites, cameras, and model types, with seedbank counts as ground truth.

Study location	Imaging platform	Weed species evaluated	Poisson AIC score	Poisson correlation (R)	NB AIC score	Negative binomial correlation (R)
Cloverland	Altum sensor	Sterile brome	36,249.12	0.1907(ns)	743.45	0.3939**
Cloverland	GoPro imagery	Common lambsquarters	12,241.26	0.0947(ns)	459.17	0.0789(ns)
Cloverland	GoPro imagery	Sterile brome	35,972.90	0.1903(ns)	736.52	0.1949(ns)
Cloverland	WorldView imagery	Common lambsquarters	10,233.75	0.2444(ns)	431.11	0.2676(ns)
Cloverland	WorldView imagery	Sterile brome	31,155.98	0.3788**	734.69	0.3459*
Pullman	Altum sensor	Italian rye	56,268.79	0.1698(ns)	1249.51	0.1320(ns)
Pullman	Altum sensor	Common lambsquarters	34,818.24	0.0765(ns)	1194.76	0.0416(ns)
Pullman	GoPro imagery	Italian rye	49,264.25	0.2428*	1150.12	0.2225*
Pullman	GoPro imagery	Common lambsquarters	32,466.18	−0.0751(ns)	1099.39	−0.1110(ns)
Pullman	WorldView imagery	Italian rye	55,023.35	0.2096*	1250.59	0.1823(ns)
Pullman	WorldView imagery	Common lambsquarters	35,682.79	0.0930(ns)	1194.92	0.1724(ns)
Uniontown	Altum sensor	Common lambsquarters	357,521.50	0.4528***	1755.66	0.4697***
Uniontown	Altum sensor	Wild oat	114,635.00	0.3226**	1533.70	0.3223**
Uniontown	GoPro imagery	Common lambsquarters	178,968.70	0.3074*	882.86	0.3012*
Uniontown	GoPro imagery	Wild oat	67,206.74	0.1779(ns)	778.40	0.1925(ns)

© 2022 The Author(s). | Published by Agro Intelligence Research Press

Uniontown	WorldView imagery	Common lambsquarters	421,041.50	0.0157(ns)	1782.33	0.0002(ns)
Uniontown	WorldView imagery	Wild oat	133,572.4	0.2567*	1553.97	0.2594**

*** = P < 0.001; ** = P < 0.01; * = P < 0.05; (ns) = not significant; NB = negative binomial. Weeds referred to by common names: common lambsquarters (*Chenopodium album* L.), cheatgrass (*Bromus tectorum* L.), Italian ryegrass (*Lolium perenne* L. ssp. *multiflorum* (Lam.) Husnot), sterile brome (*Bromus sterilis* L.), prickly lettuce (*Lactuca serriola* L.), and wild oat (*Avena fatua* L.).

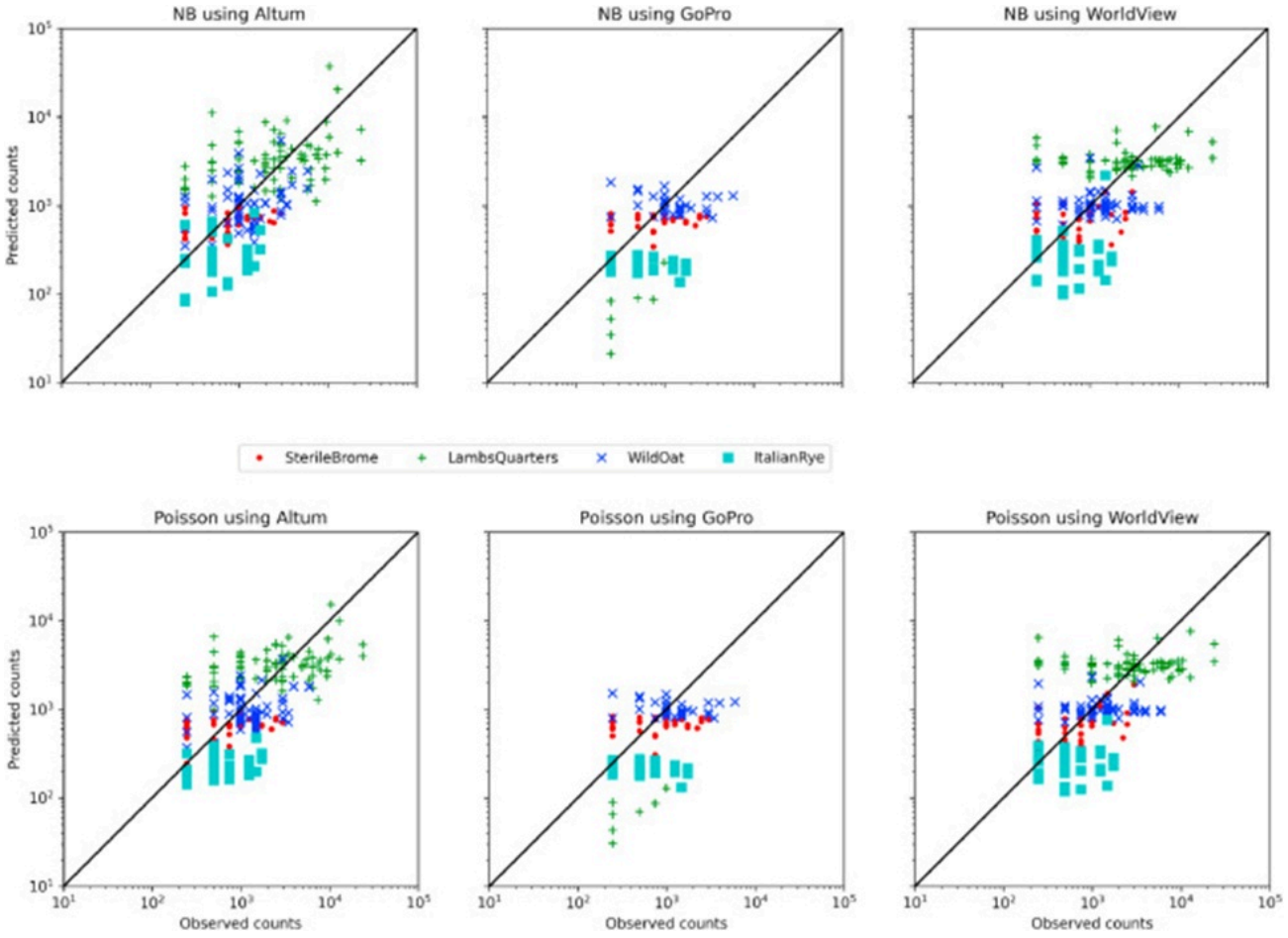

Figure 7. Prediction performance for different weeds, cameras, and count models using seedbank counts. NB: negative binomial. Weeds referred to by common names: common lambsquarters (*Chenopodium album* L.), Italian ryegrass (*Lolium perenne* L. ssp. *multiflorum* (Lam.) Husnot), sterile brome (*Bromus sterilis* L.), and wild oat (*Avena fatua* L.).

An overarching side-by-side assessment of each mapping pipeline, collapsing across weed identity, appears in **Table 6**. R values attained strong significance (P < 0.001) in every case. According to Spearman's rank correlation, Poisson models trained on Altum-PT and WorldView-2 imagery achieved optimal results when based on quadrat counts. Still, the selection of model type and sensor platform should be tailored to weed growth form—clustering species may align most naturally with NB and WorldView. In contrast, other taxa may respond better to Poisson and Altum-PT.

Table 6. Summary of model performance across ground truths and imaging platforms.

© 2022 The Author(s). | Published by Agro Intelligence Research Press

Type	Model	Ground truth	R
Altum	NB	Quadrats	0.9106***
Altum	NB	Seedbank	0.5609***
Altum	Poisson	Quadrats	0.8784***
Altum	Poisson	Seedbank	0.5676***
GoPro	NB	Quadrats	0.7004***
GoPro	NB	Seedbank	0.5122***
GoPro	Poisson	Quadrats	0.7069***
GoPro	Poisson	Seedbank	0.5210***
Parrot	NB	Quadrats	0.4351***
Parrot	Poisson	Quadrats	0.4289***
WorldView	NB	Quadrats	0.8882***
WorldView	NB	Seedbank	0.5559***
WorldView	Poisson	Quadrats	0.8607***
WorldView	Poisson	Seedbank	0.5624***

*** = P < 0.001; ** = P < 0.01; * = P < 0.05; (ns) = not significant; NB = negative binomial.

In a final step, well-fitting models—judged by R and AIC—were deployed to construct continuous weed maps. Italian ryegrass density estimated via WorldView and the NB framework at the Pullman location reveals extensive, conspicuous clusters. However, aboveground measurements trace sharper boundaries separating zones of elevated and suppressed weed density **(Figure 8)**.

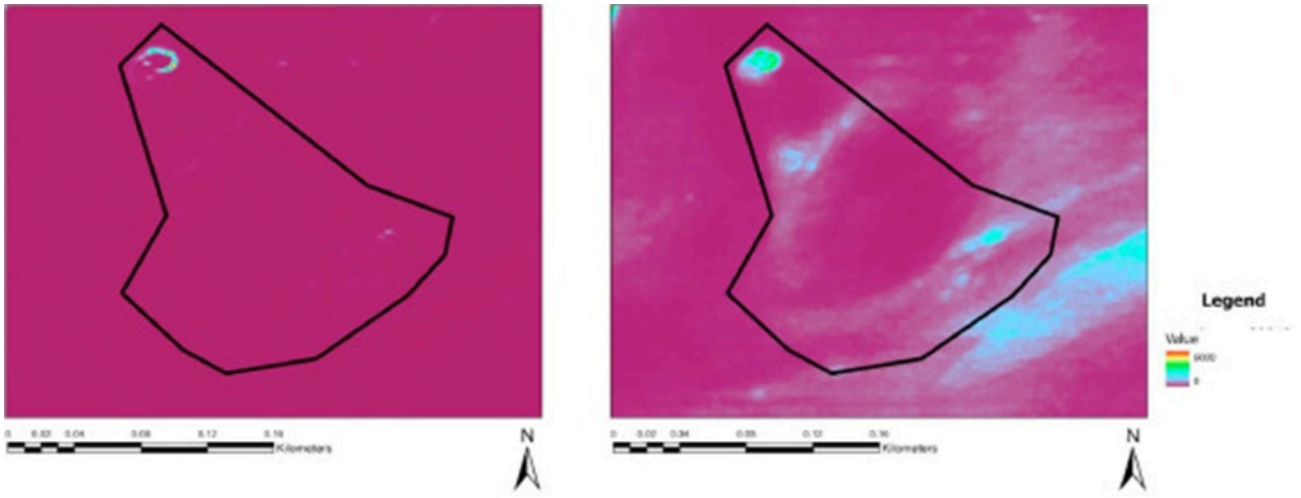

Figure 8. Aboveground Italian ryegrass (*Lolium perenne* L. ssp. *multiflorum* (Lam.) Husnot) plant density (left) and seedbank density (right) as mapped using the NB model with WorldView from the Pullman site.

While no study provides a counterpart to the present work, several related efforts documented in separate publications merit attention. Recent research has weighed the relative value of satellite against UAV platforms for detecting Canada thistle (*Cirsium arvense* L.), suggesting UAVs may be better suited to site-specific intervention [42]. That investigation,

© 2022 The Author(s). | Published by Agro Intelligence Research Press

however, restricted its scope to pre-plant weed flushes, which pose fewer identification challenges. A further review article evaluates the practicality and performance of diverse remote weed mapping strategies, synthesizing findings from multiple studies and sensor configurations. Its authors judged that the financial outlay and technical acumen required for UAV operation hinder widespread adoption and underscored the need to converge on standardized methodologies [43].

Regarding seedbanks, no published accounts link remote or proximal sensing directly to seedbank parameters. However, efforts to refine spatial sampling designs [44] informed by weed growth dynamics and management history do appear. Benoit *et al.* [45] linked seedbank maps to auxiliary variables such as soil class and management regime, suggesting a path toward more efficient seedbank sampling.

Conclusion

This paper documents the capabilities of several remote sensing weed-mapping pipelines for row crops across a range of PNW environments. The comparison underscores the indispensability of high-fidelity multispectral imagery for accurately charting weed distributions. Both the negative binomial and Poisson models performed well, routinely attaining Spearman's rank correlation coefficients of 0.8 or higher when image-derived features were used as predictors. Poisson formulations may be fitting in circumstances of limited dispersion, i.e., where weeds do not coalesce into obvious clusters. Seedbank density and quadrat-based density both represent defensible ground truth modalities for calibrating imagery. Yet, each illuminates a separate dimension of weed population structure, and seedbank data are less faithfully mapped by imagery or less strongly reflected in aboveground density readings. While aboveground assessment and remote imaging are more straightforward and less labor-intensive, seedbank characterization should be viewed as an essential and complementary metric, since soil zones rich in seeds may remain predisposed to sustained high weed pressure for years ahead. The results reported here can steer future sampling designs and guide protocols for accelerated weed mapping through remote sensing. Strikingly, seedbank tallies and aboveground counts did not correlate tightly. In forthcoming sampling initiatives, seedbank and seedling grids will be unified to resolve cross-covariograms better, thereby bridging these two population expressions. Moreover, the impressive accuracy yet limited deployability of the multispectral quadcopter setup argues for exploring a more producer-accessible configuration: namely, a lower-cost, fixed-wing drone carrying a modestly less capable sensor. Additional inquiry is required to clarify the modulating roles of topographic and edaphic variables.

Acknowledgements

This research used resources provided by the SCINet project of the USDA Agricultural Research Service, ARS project number 0500–00093–001–00-D. The authors would also like to thank Mr. Doug Finkelnburg, Ms. Jess Kalin, Ms. Marija Savic, Mr. Ian Leslie, Mr. Zachary Smith, and Mrs. Dannielle Beringer for their help in field data collection. The authors would also like to thank the producers: Mr. Joe Limbaugh, Mr. Dale Druffel, Mr. Dennis Crain, Mr. Bill Tee, Mr. Mark Greene, and Mr. Garrett Moon. This project used resources provided by PNW Herbicide Resistant Weeds Initiative (ARS Project 2090–11000–010–010-S), and the SCINet project of the USDA ARS. This research was a contribution from the Long-Term Agroecosystem Research (LTAR) network. The USDA supports LTAR.

Conflict of interest

The authors declare the following financial interests/personal relationships which may be considered as potential competing interests: This project used resources provided by PNW Herbicide Resistant Weeds Initiative (ARS Project 2090–11,000–010–010-S), Long-Term Agroecosystem Research (LTAR) for Dryland Cropping Systems of the Northwest (2090–11,000–010–023-S), and the SCINet project of the USDA ARS.

© 2022 The Author(s). | Published by Agro Intelligence Research Press

Financial support

None

Ethics statement

None

Received: 30 Aug 2021 Revised: 04 Nov 2021 Accepted: 19 Nov 2021
Published online: 25 May 2022

Rights and permissions

Open Access The author(s) retain copyright. This article is licensed under the Creative Commons Attribution-NonCommercial-ShareAlike 4.0 International License. It may be shared and adapted for non-commercial purposes with appropriate attribution, an indication of changes, and distribution of adaptations under the same license. Third-party material may be subject to separate terms identified in its credit line. View the license at https://creativecommons.org/licenses/by-nc-sa/4.0/.

References

1. Brunharo CA, Gast R, Kumar V, Mallory-Smith CA, Tidemann BD, Beckie HJ. Western United States and Canada perspective: Are herbicide-resistant crops the solution to herbicide-resistant weeds? Weed Sci. 2022;70(3):272-86. https://doi.org/10.1017/wsc.2022.6.

2. Mallory-Smith CA, Retzinger EJ. Revised classification of herbicides by site of action for weed resistance management strategies. Weed Technol. 2003;17(3):605-19. [0605:RCOHBS]2.0.CO;2 https://doi.org/10.1614/0890-037X(2003)017.

3. Zuger RJ, Burke IC. Testing in Washington identifies widespread postemergence herbicide resistance in annual grasses. Crops Soils. 2020:13-9. https://doi.org/10.1002/crso.20068.

4. San Martín C, Thorne M, Gourlie J, Lyon D, Barroso J. Seed retention of grass weeds at wheat harvest in the Pacific Northwest. Weed Sci. 2021;69(2):238-46.

5. Osipitan OA, Dille JA, Assefa Y, Knezevic SZ. Cover crop for early season weed suppression in crops: systematic review and meta-analysis. Agron J. 2018;110(6):2211-21. https://doi.org/10.2134/agronj2017.12.0752.

6. Čepl J, Kasal P. Weed mapping—a way to reduce herbicide doses. Potato Res. 2010;53:359-71.

7. Kaivosoja J, Hautsalo J, Heikkinen J, Hiltunen L, Ruuttunen P, Näsi R, et al. Reference measurements in developing UAV systems for detecting pests, weeds, and diseases. Remote Sens. 2021;13(7): 1238. https://doi.org/10.3390/rs13071238.

8. Rew LJ, Cousens RD. Spatial distribution of weeds in arable crops: Are current sampling and analytical methods appropriate? Weed Res. 2001;41(1):1-18. https://doi.org/10.1046/j.1365-3180.2001.00215.x.

9. Brix A, Andreasen C. The relation between densities and frequencies of weeds in arable fields. J Agric Biol Environ Stat. 2000:372-86. https://doi.org/10.2307/1400460.

10. Ambrosio L, Iglesias L, Marin C, Del Monte JP. Evaluation of sampling methods and assessment of the sample size to estimate the weed seedbank in soil, taking into account spatial variability. Weed Res. 2004;44(3):224-36.

11. Mortensen DA, Johnson GA, Young LJ. Weed distribution in agricultural fields. Proceedings of soil specific crop management: a workshop on research and development issues. American Society of Agronomy, Crop Science Society of America, Soil Science Society of America, Madison, WI. 1993:113-24.

12. Metcalfe H, Milne AE, Webster R, Lark RM, Murdoch AJ, Storkey J. Designing a sampling scheme to reveal correlations between weeds and soil properties at multiple spatial scales. Weed Res. 2016;56(1):1-13.

13. López-Granados FT-S, De Castro AI, Serrano-Pérez A, Mesas-Carrascosa FJ, Peña JM. Object-based early monitoring of a grass weed in a grass crop using high resolution UAV imagery. Agron Sustain Dev. 2016;36:1-12. https://doi.org/10.1007/s13593-016-0405-7.

14. Agarwal R, Hariharan S, Rao MN, Agarwal A. Weed identification using K-Means clustering with color spaces features in multi-spectral images taken by UAV. 2021 IEEE International Geoscience and Remote Sensing Symposium IGARSS. IEEE. 2021:7047-50.

15. Ajayi OG, Ashi J, Guda B. Performance evaluation of YOLO v5 model for automatic crop and weed classification on UAV images. Smart Agric Technol. 2023;5: 100231. https://doi.org/10.1016/j.atech.2023.100231.

16. Rai N, Sun X. WeedVision: A single-stage deep learning architecture to perform weed detection and segmentation using drone-acquired images. Comput Electron Agric. 2024;219:108792. https://doi.org/10.1016/j.compag.2024.108792.

17. Rehman MU, Eesaar H, Abbas Z, Seneviratne L, Hussain I, Chong KT. Advanced drone-based weed detection using feature-enriched deep learning approach. Knowl Based Syst. 2024;305:112655. https://doi.org/10.1016/j.knosys.2024.112655.

18. Vayssade JA, Jones G, Paoli JN. Towards the characterization of crop and weeds at leaf scale: a large comparison of shape, spatial and textural features. Smart Agric Technol. 2023;5:100245. https://doi.org/10.1016/j.atech.2023.100245.

19. National Centers for Environmental Information, U.S. Climate Normals. https://www.ncei.noaa.gov/access/us-climate-normals. 2024.

20. OpenDroneMap Authors. ODM – A command line toolkit to generate maps, point clouds, 3D models and DEMs from drone, balloon or kite images, Retrieved from OpenDroneMap/ODM GitHub Page. https://github.com/OpenDroneMap/ODM. 2020.

21. Pix4DSA. PIX4Dfields (2.5.0) [Software]. Prilly, Switzerland. 2024. https://www.pix4d.com/product/pix4dfields/

22. Canon. EOS REBEL T100, EOS 3000D [Apparatus]. Ota City, Tokyo, Japan. 2024. https://www.csai.canon.com/support/p/eos-rebel-t100

23. Roboflow Inc. Roboflow - Computer Vision Tools For Developers and Enterprises, Roboflow . 2024. https://roboflow.com/

24. R-Tech Industries. Elutriator 48-X [Apparatus]. Homewood, MB, Canada. 2024. https://www.r-techind.com/elutriator.

25. Delorit R. Illustrated taxonomy manual of weed seeds. 1970.

© 2022 The Author(s). | Published by Agro Intelligence Research Press

26. Margaret G, Dennis La Rea J. Gilkey's weeds of the Pacific Northwest. Rev. 1980.

27. Dessaint F, Barralis G, Caixinhas M, Mayor J, Recasens J, Zanin G. Precision of soil seedbank sampling: how many soil cores? Weed Res. 1996;36(2):143-51. https://doi.org/10.1111/j.1365-3180.1996.tb01810.x.

28. Parrot. Parrot Anafi [Apparatus]. Paris, France.20220. https://www.parrot.com/assets/s3fs-public/2021-09/anafi-user-guide.pdf.

29. GoPro. Hero 10 Black [Apparatus]. San Mateo, CA, USA. 2021. https://gopro.com/content/dam/help/hero10-black/manuals/HERO10Black_UM_ENG_REVB.pdf.

30. Aerial Technology International. ATI Bot v2 [Apparatus]. Clackamas, OR, USA. 2024. https://www.aerialtechnology.com/bot.

31. AgEagle Aerial Systems. Altum-PT [Apparatus]. Wichita, KS, USA. 2024. https://ageagle.com/drone-sensors/altum-pt-camera/

32. Environmental Systems Research Institute. ArcGIS (3.2) [Software]. Redlands, CA, USA. 2023. https://www.esri.com/en-us/arcgis/products/arcgis-pro/overview

33. European Space Agency. WorldView-2. 2024. https://earth.esa.int/eogateway/missions/worldview-2

34. Laben CA, Brower BV. Process for enhancing the spatial resolution of multispectral imagery using pan-sharpening. U.S. Patent 6,011,875. 2000.

35. SDA. SCINet Home. 2024. https://scinet.usda.gov

36. Pedregosa F, Varoquaux G, Gramfort A, Michel V, Thirion B, Grisel O, et al. Scikit-learn: machine learning in Python. J Mach Learn Res. 2011;12:2825-30.

37. Van Rossum G, Drake FL. Python 3 Reference Manual. Scotts Valley, CA: CreateSpace; 2009.

38. Seabold S, Perktold J. statsmodels: econometric and statistical modeling with Python. Proceedings of the 9th Python in Science Conference. 2010.

39. Corteva Agriscience. Rioxarray (0.15.7) [Software]. Indianapolis, IN, USA. 2024. https://corteva.github.io/rioxarray/html/readme.html

40. Menalled F, Gross K, Hammond M. Weed aboveground and seedbank community responses to agricultural management systems. Ecol Appl. 2001;11(6):1586-601. [1586:WAASCR]2.0.CO;2 https://doi.org/10.1890/1051-0761(2001)011.

41. Cardina J, Sparrow DH, McCoy EL. Spatial relationships between seedbank and seedling populations of common lambsquarters (Chenopodium album) and annual grasses. Weed Sci. 1996;44(2):298-308. https://doi.org/10.1017/S0043174500093929.

42. Rasmussen J, Azim S, Nielsen J. Pre-harvest weed mapping of Cirsium arvense L. based on free satellite imagery–The importance of weed aggregation and image resolution. Eur J Agron. 2021;130: 126373. https://doi.org/10.1016/j.eja.2021.126373.

43. López-Granados F. Weed detection for site-specific weed management: mapping and real-time approaches. Weed Res. 2011;51(1):1-11. https://doi.org/10.1111/j.1365-3180.2010.00829.x.

© 2022 The Author(s). | Published by Agro Intelligence Research Press

44. Wiles L, Schweizer E. Spatial dependence of weed seed banks and strategies for sampling. Weed Sci. 2002;50(5):595-606. [0595:SDOWSB]2.0.CO;2
https://doi.org/10.1614/0043-1745(2002)050.

45. Benoit DL, Derksen DA, Panneton B. Innovative approaches to seedbank studies. Weed Sci. 1992;40(4):660-9.
https://doi.org/10.1017/S0043174500058276.

© 2022 The Author(s). | Published by Agro Intelligence Research Press